ACADEMIC PRESS

Available online at www.sciencedirect.com

SCIENCE DIRECT®

Journal of Sound and Vibration 262 (2003) 889–906

JOURNAL OF SOUND AND VIBRATION

www.elsevier.com/locate/jsvi

Identification of a continuous structure with a geometrical non-linearity. Part I: Conditioned reverse path method

G. Kerschen*, V. Lenaerts, J.-C. Golinval

LTAS—Vibrations et Identification des Structures, Université de Liège, Chemin des Chevreuils 1 (B52), B-4000 Liège, Belgium

Received 12 October 2001; accepted 8 April 2002

Abstract

Particular effort has been spent in the field of identification of multi-degree-of-freedom non-linear systems. The newly developed methods permit the structural analyst to consider increasingly complex systems. The aim of this paper and a companion paper is to study, by means of two methods, a continuous non-linear system consisting of an experimental cantilever beam with a geometrical non-linearity. In this paper (Part I), the ability of the conditioned reverse path method, which is a frequency domain technique, to identify the behaviour of this structure is assessed. The companion paper (Part II) is devoted to the application of proper orthogonal decomposition, which is an updating technique, to the test example.

1. Introduction

The last 20 years have witnessed impressive progress in non-linear structural dynamics. The identification of non-linear systems began with the study of single-degree-of-freedom (s.d.o.f.) systems. Since the reference paper of Masri and Caughey [1] in 1979, techniques which can consider multi-degree-of-freedom (m.d.o.f.) systems were introduced, e.g. the Hilbert transform [2], NARMAX models [3,4] and Volterra series [5]. However, it appeared quickly that these techniques are not suitable for systems with high modal density. For a detailed review of the past years, the reader is referred to Refs. [6,7]. Progress in the treatment of m.d.o.f. systems has been realized recently and can be attributed to a confluence of new methods of analysis and to the expansion of computer processor power.

*Corresponding author. Fax: +32-4-366-48-56.
E-mail address: g.kerschen@ulg.ac.be (G. Kerschen).

0022-460X/03/$ - see front matter
doi:10.1016/S0022-460X(02)01151-3

Proper orthogonal decomposition (POD), also known as principal component analysis or Karhunen–Loève transform, has shown promise for model updating of structural parameters in m.d.o.f. non-linear systems [8,9]. The procedure is based on the solution of an optimization problem which consists in minimizing the difference between the bi-orthogonal decompositions of the measured and simulated data, respectively.

The development of frequency response function (FRF)-based approaches has received increasing attention in the last 10 years. The non-linear identification through feedback of the outputs (NIFO) exploits the spatial information and treats the non-linear forces as internal feedback forces in the underlying linear model of the system [10]. The key advantage of this method lies in its ability to estimate the FRFs of the underlying linear system and the non-linear coefficients in a single step. This is carried out in a least-squares system of equations through averaging. The concept of a reverse path (RP) model was first introduced by Rice and Fitzpatrick [11]. However, this technique requires excitation at every response location. The conditioned reverse path (CRP) formulation [12] extends the application of the RP algorithm to systems characterized by non-linearities away from the location of the applied force. This method has been developed by generalizing the concepts introduced in Refs. [11,13,14]. Conditioned frequency responses are computed and yield the underlying linear properties without influence of non-linearities. The non-linear coefficients are identified in a second step.

As stated in Ref. [6], researchers often concentrate too much on lumped parameter systems and many techniques collapse when faced with systems with a higher modal density. In this paper and a companion paper [15], it is proposed to study by means of two methods a continuous non-linear system consisting of an experimental cantilever beam with a geometrical non-linearity. In this paper (Part I), the ability of the CRP method to identify the behaviour of this structure is assessed. The companion paper (Part II) is devoted to the application of POD to the test example.

2. CRP method

In the presence of non-linear forces, the classical H_1 and H_2 estimators [16] should not be used because the non-linearities corrupt the underlying linear characteristics of the response. In the CRP method, spectral conditioning techniques are exploited to remove the effects of non-linearities before computing the FRFs of the underlying linear system. Once the FRFs are known, the non-linear coefficients may then be evaluated.

In the following, the notations match the ones used in Ref. [12]. The vibrations of a general non-linear system are governed by equation

$$\mathbf{M}\ddot{\mathbf{x}}(t) + \mathbf{C}\dot{\mathbf{x}}(t) + \mathbf{K}\mathbf{x}(t) + \sum_{j=1}^{n} \mathbf{A}_j \mathbf{y}_j(t) = \mathbf{f}(t), \tag{1}$$

where $\mathbf{y}_j(t)$ is a non-linear function vector and $\mathbf{A}_j$ contains the coefficients of the non-linear terms $\mathbf{y}_j(t)$. In the frequency domain, Eq. (1) becomes

$$\mathbf{B}(\omega)\mathbf{X}(\omega) + \sum_{j=1}^{n} \mathbf{A}_j \mathbf{Y}_j(\omega) = \mathbf{F}(\omega), \tag{2}$$

where $\mathbf{X}(\omega), \mathbf{Y}_j(\omega)$ and $\mathbf{F}(\omega)$ are the Fourier transforms of $\mathbf{x}(t), \mathbf{y}_j(t)$ and $\mathbf{f}(t)$ and $\mathbf{B}(\omega) = (-\omega^2\mathbf{M} + \mathrm{i}\omega\mathbf{C} + \mathbf{K})$ is the linear dynamic stiffness matrix.

By imposing the applied force to be the output and the measured responses to be the inputs, a reverse path (RP) model is constructed (Fig. 1). For the sake of brevity, the RP formulation is not recalled here. For a detailed description of this technique, the reader is referred to Ref. [12].

2.1. Estimation of the underlying linear system properties

The key concept of the CRP formulation is the separation of the non-linear part of the system response from the linear part and the construction of uncorrelated response components in the frequency domain.

The spectra of the measured responses $\mathbf{X}$ can be decomposed into a component which is correlated with the spectrum of the first non-linear vector $\mathbf{Y}_1$, denoted by $\mathbf{X}_{(+1)}$, through a frequency response matrix $\mathbf{L}_{1X}$, and a component which is uncorrelated with the spectrum of the non-linear vector, denoted by $\mathbf{X}_{(-1)}$ (Fig. 2). The spectral component $\mathbf{X}_{(-1:n)}$ is the component of the response uncorrelated with the spectra of all n non-linear function vectors and may be viewed as the response of the underlying linear system

$$\mathbf{X}_{(-1:n)} = \mathbf{X} - \sum_{j=1}^{n} \mathbf{X}_{(+j)} = \mathbf{X} - \sum_{j=1}^{n} \mathbf{L}_{jX}\mathbf{Y}_{j(-1:j-1)}. \tag{3}$$

The reverse path model of Fig. 1 can now be replaced by the reverse path model of Fig. 3 where the inputs are uncorrelated. This latter figure shows that the path between $\mathbf{X}_{(-1:n)}$ and $\mathbf{F}_{(-1:n)}$ is the

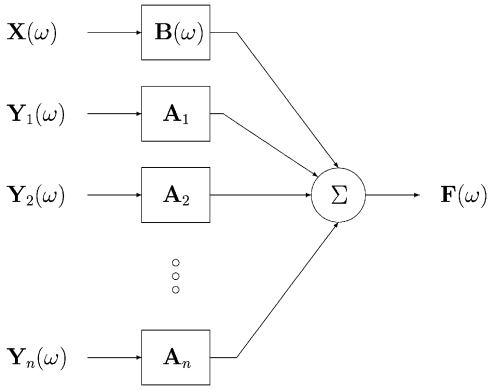

Fig. 1. Reverse path model.

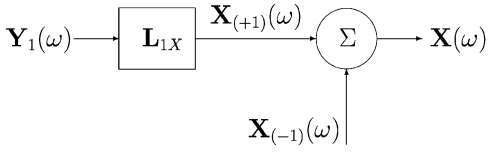

Fig. 2. Decomposition of the spectra of the measured responses.

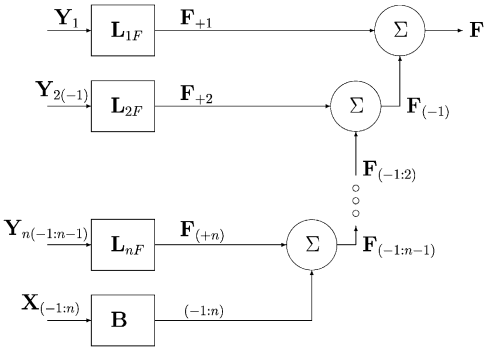

Fig. 3. Reverse path model with uncorrelated inputs.

linear dynamic stiffness matrix $\mathbf{B}$

$$\mathbf{F}_{(-1:n)}(\omega) = \mathbf{B}(\omega)\mathbf{X}_{(-1:n)}(\omega). \tag{4}$$

By transposing Eq. (4), pre-multiplying by the complex conjugate of $\mathbf{X}$, noted $\mathbf{X}^*$, taking the expectation and finally multiplying by $2/T$, the underlying linear system may be identified without corruption from the non-linear terms

$$\begin{aligned}\mathbf{G}_{XF(-1:n)} &= \frac{2}{T} E[\mathbf{X}^*\mathbf{F}^{\mathrm{T}}_{(-1:n)}] = \frac{2}{T} E[\mathbf{X}^*(\mathbf{B}\mathbf{X}_{(-1:n)})^{\mathrm{T}}] \\ &= \frac{2}{T} E[\mathbf{X}^*\mathbf{X}^{\mathrm{T}}_{(-1:n)}\mathbf{B}^{\mathrm{T}}] = \mathbf{G}_{XX(-1:n)}\mathbf{B}^{\mathrm{T}},\end{aligned} \tag{5}$$

where $\mathbf{G}_{XF(-1:n)}$ and $\mathbf{G}_{XX(-1:n)}$ are conditioned power spectral density matrices.

For the dynamic compliance matrix $\mathbf{H}$,

$$H_{c2} : \mathbf{H}^{\mathrm{T}} = \mathbf{G}^{-1}_{XF(-1:n)}\mathbf{G}_{XX(-1:n)}. \tag{6}$$

This expression is known as the conditioned H_{c2} estimate. If Eq. (4) is multiplied by the complex conjugate of $\mathbf{F}$, the conditioned H_{c1} is obtained

$$H_{c1} : \mathbf{H}^{\mathrm{T}} = \mathbf{G}^{-1}_{FF(-1:n)}\mathbf{G}_{FX(-1:n)}. \tag{7}$$

2.2. Estimation of the non-linear coefficients

Once the linear dynamic compliance $\mathbf{H}$ is identified, the non-linear coefficients $\mathbf{A}_j$ may be estimated. Using the same procedure as for Eq. (5), the following relationship is obtained:

$$\mathbf{G}_{iF(-1:i-1)} = \mathbf{G}_{iX(-1:i-1)}\mathbf{B}^{\mathrm{T}} + \sum_{j=1}^{n} \mathbf{G}_{ij(-1:i-1)}\mathbf{A}_j^{\mathrm{T}}. \tag{8}$$

It should be noted that $\mathbf{G}_{ij(-1:i-1)} = E[\mathbf{Y}^*_{i(-1:i-1)}\mathbf{Y}_j^{\mathrm{T}}] = \mathbf{0}$ for $j<i$ since $\mathbf{Y}^*_{i(-1:i-1)}$ is uncorrelated with the spectra of the non-linear function vectors $\mathbf{Y}_1$ through $\mathbf{Y}_{i-1}$. If Eq. (8) is pre-multiplied by $\mathbf{G}^{-1}_{ii(-1:i-1)}$, the first term in the summation is $\mathbf{A}_i^{\mathrm{T}}$. Finally,

$$\mathbf{A}_i^{\mathrm{T}} = \mathbf{G}^{-1}_{ii(-1:i-1)}\left(\mathbf{G}_{iF(-1:i-1)} - \mathbf{G}_{iX(-1:i-1)}\mathbf{B}^{\mathrm{T}} - \sum_{j=i+1}^{n} \mathbf{G}_{ij(-1:i-1)}\mathbf{A}_j^{\mathrm{T}}\right). \tag{9}$$

The identification process starts with the computation of $\mathbf{A}_n$ working backwards to $\mathbf{A}_1$. At this stage, it is important to emphasise that the non-linear coefficients are frequency dependent. However, by taking the spectral mean, the actual value of the coefficients may be retrieved.

It can be shown [17] that conditioned power spectral density matrices like $\mathbf{G}_{XF(-1:n)}$ may be obtained from

$$\mathbf{G}_{ij(-1:r)} = \mathbf{G}_{ij(-1:r-1)} - \mathbf{G}_{ir(-1:r-1)}\mathbf{L}_{rj}^{\mathrm{T}}, \tag{10}$$

where

$$\mathbf{L}_{rj}^{\mathrm{T}} = \mathbf{G}_{rr(-1:r-1)}^{-1}\mathbf{G}_{rj(-1:r-1)}. \tag{11}$$

2.3. Coherence functions

For linear systems, the ordinary coherence function is a means to assess the quality of transfer function estimates [16]. However, for a multiple input model with correlated inputs, the sum of ordinary coherences between the inputs and the output may be greater than unity. In Ref. [18], the concept of ordinary coherence function is replaced by the concept of cumulative coherence function γ_{Mi}^2

$$\gamma_{Mi}^2(\omega) = \gamma_{X_iF(-1:n)}^2(\omega) + \gamma_{YF}^2(\omega) = \gamma_{X_iF(-1:n)}^2(\omega) + \sum_{j=1}^{n} \gamma_{jF(-1:j-1)}^2(\omega), \tag{12}$$

where

- $\gamma_{X_iF(-1:n)}^2$ is the ordinary coherence function between the ith element of $X_{(-1:n)}$ and excitation F

$$\gamma_{X_iF(-1:n)}^2 = \frac{|G_{X_iF(-1:n)}|^2}{G_{X_iX_i(-1:n)}G_{FF}} \tag{13}$$

  and indicates the contribution from the linear spectral component of the response of the ith output.
- $\gamma_{jF(-1:j-1)}^2$ is the ordinary coherence function between the conditioned spectrum $Y_{j(-1:j-1)}$ and excitation F

$$\gamma_{jF(-1:j-1)}^2 = \frac{|G_{jF(-1:j-1)}|^2}{G_{jj_{(-1:j-1)}}G_{FF}} \tag{14}$$

  and $\sum_{j=1}^{n} \gamma_{jF(-1:j-1)}^2$ indicates the contribution from the non-linearities.

The cumulative coherence function is always between 0 and 1 and may be considered as a measure of the accuracy of the model.

3. Experimental set-up

The benchmark is similar to the one proposed by the Ecole Centrale de Lyon (France) in the framework of COST Action F3 working group on "Identification of non-linear systems" [19].

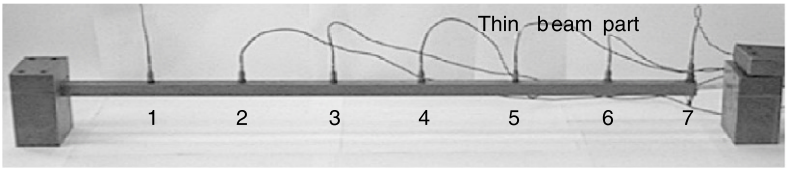

Fig. 4. Experimental set-up.

Table 1
Geometrical and mechanical properties of the set-up

	Length (m)	Width (m)	Thickness (m)	Material
Main beam	0.7	0.014	0.014	Steel
Thin beam part	0.04	0.014	0.0005	Steel

This experimental application involves a clamped beam with a thin beam part at the end of the main beam (Fig. 4). The geometrical and mechanical properties of the set-up are listed in Table 1.

Seven accelerometers which span the beam regularly are used to measure the response and in addition a displacement sensor is also located at the end of the beam, i.e., at position 7. The excitation force is white-noise sequence band limited in the 0–500 Hz range. Due to the thin beam part, the effect of gravity is not negligible. Accordingly, two different set-ups are considered:

- the *horizontal set-up* in which the thin part is horizontal and the shaker, located at position 2, excites the structure in a vertical plane (see Fig. 5(a)).
- the *vertical set-up* in which the thin part is vertical and the shaker, located at position 3, excites the structure in a horizontal plane (see Fig. 5(b)).

4. Identification results: horizontal set-up

4.1. Conventional frequency response estimation (H_2 estimate)

Different excitation levels are considered in the 0.3–21 N r.m.s. range. In order to have some ideas about the influence of the non-linearity, the FRFs are first estimated using the classical H_2 method. Fig. 6 illustrates the magnitude of H_{72} for the lowest (0.3 N r.m.s.) and highest (21 N r.m.s.) excitation levels. As can be seen in this figure, distortions appear in the FRF when the excitation level is increased. This is confirmed by the ordinary coherence functions (Fig. 7). Accordingly, if the structure may be assumed to be linear for the lowest excitation level, it is no longer the case for higher levels. Indeed, if the excitation level is increased, the thin part is excited with a large deflection and a geometrical non-linearity is activated.

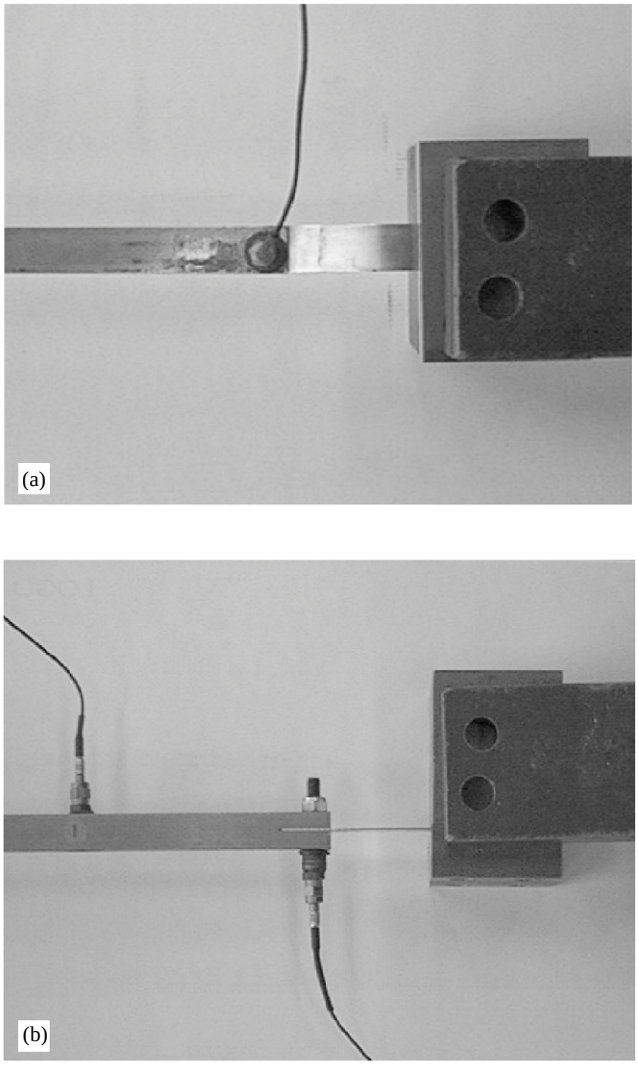

Fig. 5. Experimental set-up, above view: (a) horizontal set-up and (b) vertical set-up.

4.2. Conditioned frequency response estimation (H_{c2} estimate)

4.2.1. Model selection

The first step in the identification procedure is the model selection. With this aim, the cumulative coherence function γ^2_{Mi} as defined in Section 2.3 is exploited. Similar work [20] was done using partial and multiple coherences defined by Bendat [17].

To model the stiffening effect of the thin beam part, a grounded symmetrical non-linearity of type $|x|^{\alpha}\text{sign}(x)$ is introduced in the model at the end of the beam (location 7). Due to the presence of a second harmonic of the first mode in the FRF (Fig. 6(b)), an asymmetrical non-linearity of

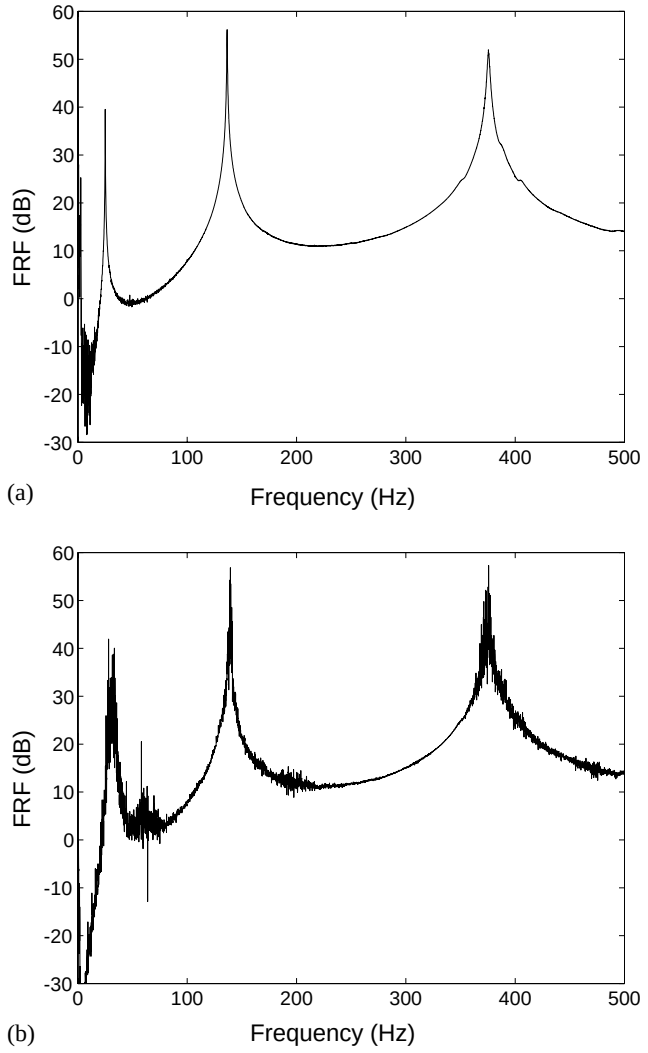

Fig. 6. Horizontal set-up, magnitude of H_{72} (H_2 estimate): (a) 0.3 N r.m.s. and (b) 21 N r.m.s.

type $|x|^{\beta}$ is added to the model. Thus, the non-linearity is modelled as

$$f(x) = A|x|^{\alpha}\text{sign}(x) + B|x|^{\beta}, \tag{15}$$

where x is the displacement at the end of the beam. Exponents α and β are determined by seeking the maximum value for the spectral mean of the averaged cumulative coherence of all the seven sensors

$$accuracy = \frac{1}{N}\sum_{\omega=10}^{500}\left(\frac{1}{7}\sum_{i=1}^{7}\gamma_{Mi}^{2}(\omega)\right), \tag{16}$$

where N is the number of frequencies considered in the range from 10 to 500 Hz. The maximum value is found for $\alpha = 3$ and $\beta = 2$ and is equal to 0.9834.

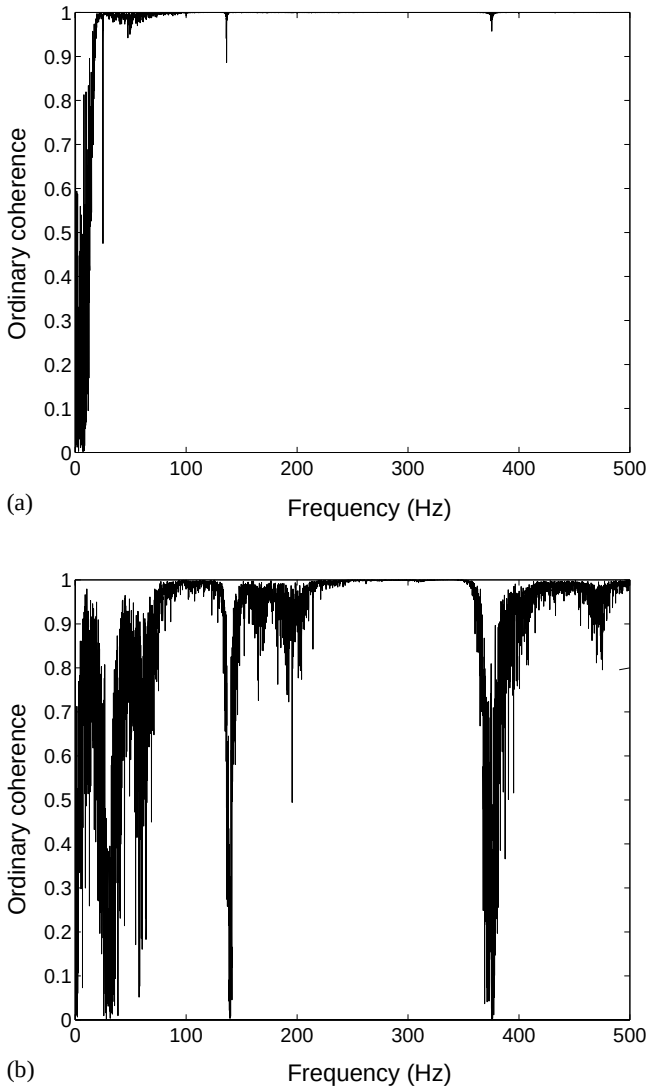

Fig. 7. Horizontal set-up, ordinary coherence functions $\gamma^2_{X_7F}$: (a) 0.3 N r.m.s. and (b) 21 N r.m.s.

4.2.2. Estimation of the FRFs of the underlying linear system

The H_{c2} estimate (6) is used to compute the FRFs of the underlying linear system. Fig. 8 illustrates the magnitude of H_{72} together with the cumulative coherence γ^2_{M7} for the 21 N r.m.s. level. Apart from a few drops (particularly around the first resonance), the cumulative coherence is unity indicating that the model is quite accurate. Fig. 9 represents the comparison between the *true* FRF, i.e., the FRF for the 0.3 N r.m.s. level, and the FRFs obtained using the H_{c2} and H_2 estimates for the first two resonances. It can clearly be seen that the H_{c2} estimate is closer to the *true* FRF while the H_2 estimate is contaminated by the presence of the non-linearity.

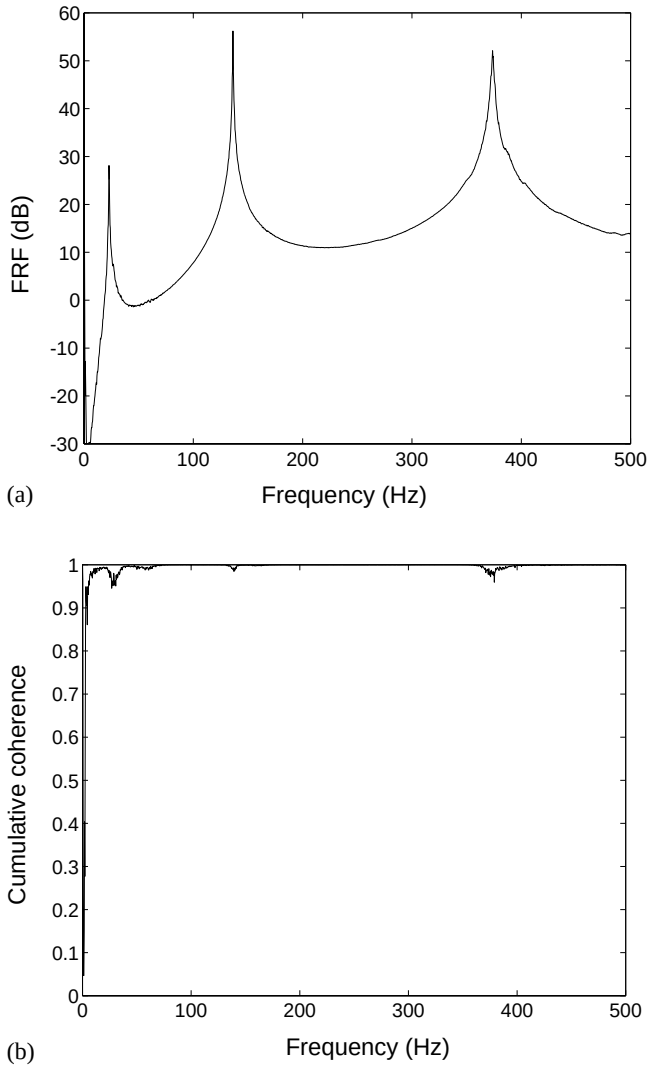

Fig. 8. Horizontal set-up, 21 N r.m.s. level: (a) magnitude of H_{72} (H_{c2} estimate) and (b) cumulative coherence γ^2_{M7}.

4.2.3. *Estimation of the non-linear coefficient*

Once the FRFs of the underlying linear system are evaluated, the non-linear coefficients may then be calculated. Fig. 10 displays the real part of the non-linear coefficients A and B (see Eq. (15)). As pointed out previously, the coefficients are frequency dependent and a spectral mean has to be performed to obtain a single value for the coefficients. From the superposition of the *true* FRF and the H_2 estimate, it can be observed that the non-linear behaviour occurs between 10 and 250 Hz. Accordingly, the spectral mean of the non-linear coefficients is realized in this range. Table 2 gives the spectral mean of A and B for the 8, 16 and 21 N r.m.s. levels. The real part of coefficient A is stable while the real part of coefficient B decreases as the level increases. It is also worth pointing out that the imaginary part of the coefficients, without any physical meaning, is several orders of magnitude below the real part.

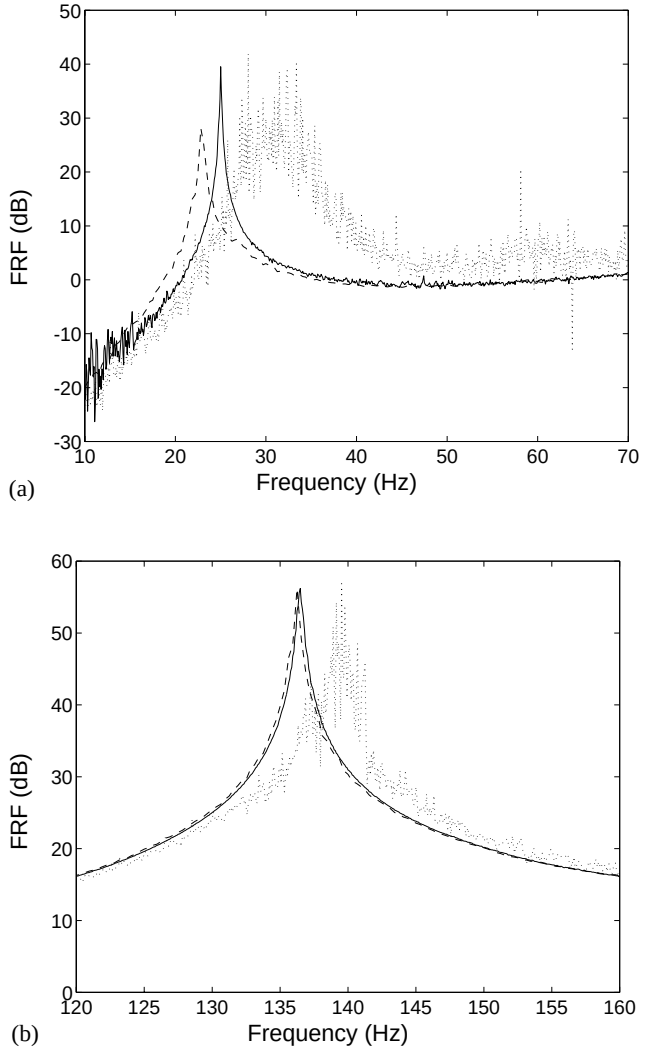

Fig. 9. Horizontal set-up, magnitude of H_{72}. —, true FRF (0.3 N r.m.s.); ⋯⋯, H_2 estimate (21 N r.m.s.); - - -, H_{c2} estimate (21 N r.m.s.): (a) first resonance and (b) second resonance.

4.3. Summary of the results

Non-linearities introduce distortions in the FRFs as can be seen with the H_2 estimate. The H_{c2} estimate allows these distortions to be removed:

- for the first resonance, the peak predicted by the CRP method is closer to the actual peak than the peak obtained with the H_2 estimate;
- for the second resonance, the H_{c2} estimate almost merges with the actual peak.

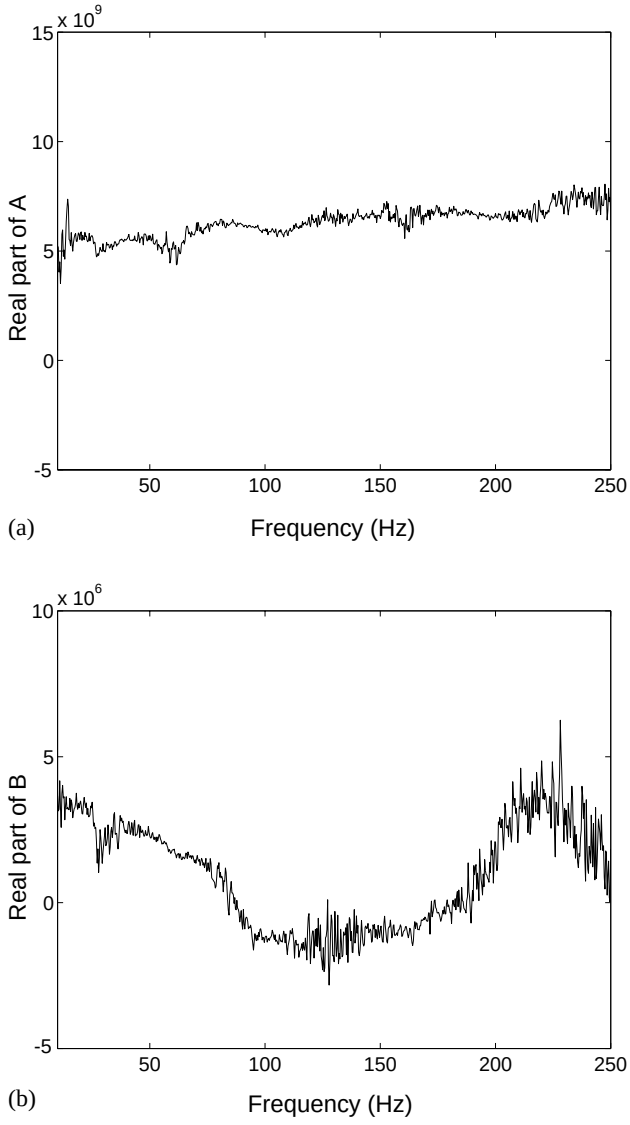

Fig. 10. Horizontal set-up, real part of the non-linear coefficients (21 N r.m.s.): (a) A and (b) B.

Table 2
Spectral mean (10–250 Hz) of the non-linear coefficients

Excitation level (N r.m.s.)	A (N/m^3)	B (N/m^2)
8	$6.65 \times 10^9 - \mathrm{i}5.30 \times 10^7$	$2.53 \times 10^6 - \mathrm{i}1.45 \times 10^4$
16	$6.41 \times 10^9 + \mathrm{i}1.26 \times 10^7$	$1.25 \times 10^6 + \mathrm{i}2.64 \times 10^4$
21	$6.29 \times 10^9 + \mathrm{i}5.31 \times 10^7$	$7.85 \times 10^5 + \mathrm{i}5.91 \times 10^4$

However, the results can be substantially improved. The second harmonic that appears in the FRF (Fig. 6(b)) is due to the influence of gravity and cannot be modelled with an asymmetrical non-linearity. This is the reason why coefficient B is found to vary strongly with frequency (Fig. 10(b)) and why its spectral mean decreases when the excitation level increases (Table 2). This may also explain why the frequency of the first resonance is not well predicted by the H_{c2} estimate.

Indeed, gravity is at the origin of a static deflection of the two beams. This deflection imposes a non-negligible pre-stress in the thin beam part which is responsible for the second harmonic in the FRF.

5. Identification results: vertical set-up

In order to reduce the influence of gravity, the vertical set-up shown in Fig. 5(b) was built. In this section, the CRP is again exploited to identify the non-linear behaviour of the thin beam part. Different excitation levels are considered in the 1.4–22 N r.m.s. range.

5.1. Conventional frequency response estimation (H_2 estimate)

Fig. 11 displays the magnitude of H_{73} for the lowest (1.4 N r.m.s.) and highest (22 N r.m.s.) excitation levels. It is worth pointing out that the structure can be considered as linear for the lowest level. In comparison with Fig. 6, the second harmonic has almost completely disappeared. To consider the influence of the non-linearity on the FRFs, the natural frequencies are estimated in the 0–500 Hz range using the least squares complex exponential (LSCE) method [16]. The results are summarized in Table 3. It can be observed that the first two natural frequencies are shifted towards higher frequencies when the excitation level is increased. This is due to the stiffening effect of the thin beam part. The third natural frequency does not seem to be affected by the presence of the non-linearity.

5.2. Conditioned frequency response estimation (H_{c2} estimate)

5.2.1. Model selection

As in Section 4.2.1, the thin beam part is modelled with a grounded symmetrical non-linearity

$$f(x) = A|x|^{\alpha}\mathrm{sign}(x). \tag{17}$$

Since, the effect of gravity is now negligible, the asymmetrical non-linearity is not included in the model. The best results in terms of spectral mean of the averaged cumulative coherence of all the sensors are obtained with $\alpha = 2.8$ (accuracy = 0.9873).

5.2.2. Estimation of the FRFs of the underlying linear system

Fig. 12 represents the magnitude of H_{73} (H_{c2} estimate) together with the cumulative coherence γ^2_{M7} for the 22 N r.m.s. level. Fig. 13 is the comparison between the *true* FRF, i.e., the FRF for the 1.4 N r.m.s. level, and the FRFs obtained using the H_{c2} and H_2 estimates for the first two resonances. The natural frequencies are also estimated from the H_{c2} estimate using LSCE method. Table 4 gives the natural frequencies identified for the different excitation levels.

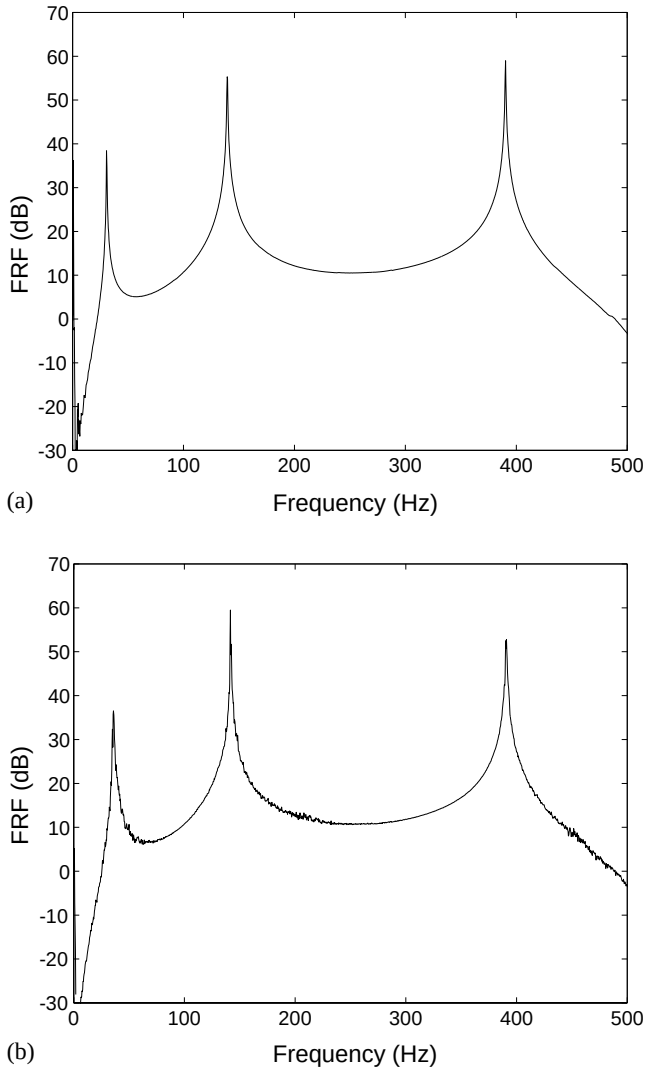

Fig. 11. Vertical set-up, magnitude of H_{73} (H_2 estimate): (a) 1.4 N r.m.s. and (b) 22 N r.m.s.

Table 3
Natural frequencies (H_2 estimate)

Excitation level (N r.m.s.)	First freq. (Hz)	Second freq. (Hz)	Third freq. (Hz)
1.4	30.74	139.47	390.22
2.8	30.99	139.49	390.16
5.5	31.60	139.64	390.12
11	33.13	140.29	390.17
16	34.81	140.84	390.34
22	36.80	141.80	390.54

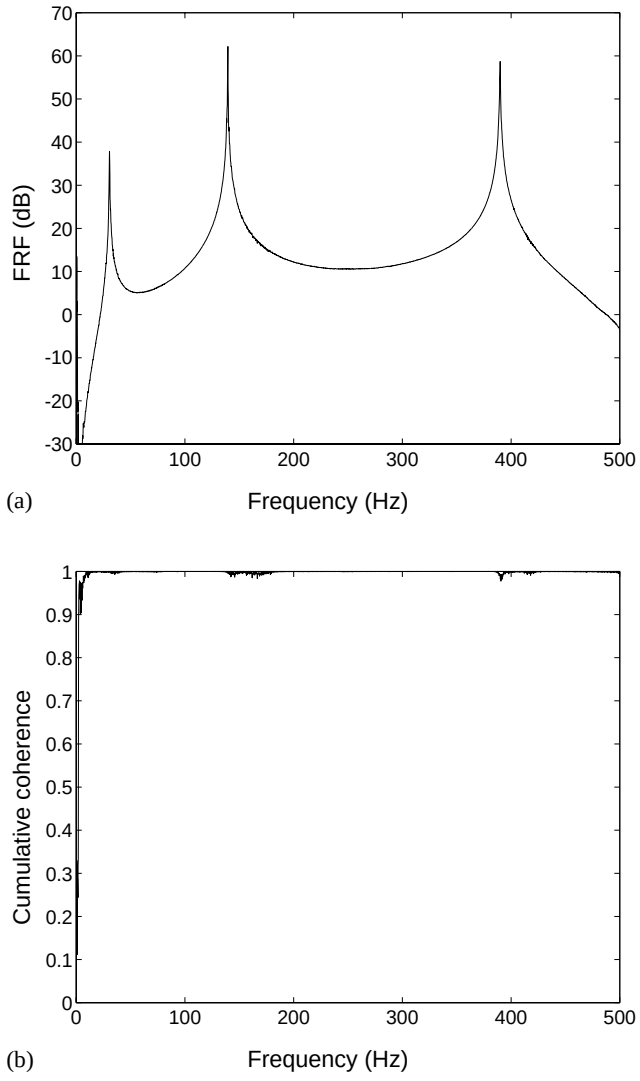

Fig. 12. Vertical set-up, 22 N r.m.s. level: (a) magnitude of H_{73} (H_{c2} estimate) and (b) cumulative coherence γ^2_{M7}.

Appreciable results have been obtained. For instance, in comparison with the horizontal set-up, the natural frequency of the first mode is now well estimated.

5.2.3. Estimation of the non-linear coefficient

The last step of the identification procedure is the computation of the non-linear coefficient. Fig. 14 represents the real part of coefficient A and the spectral mean (10–250 Hz) of this coefficient for all excitation levels is listed in Table 5. Apart from the 2.8 and 5.5 N r.m.s. levels for which the non-linearity does not participate sufficiently in the system response, a stable value for

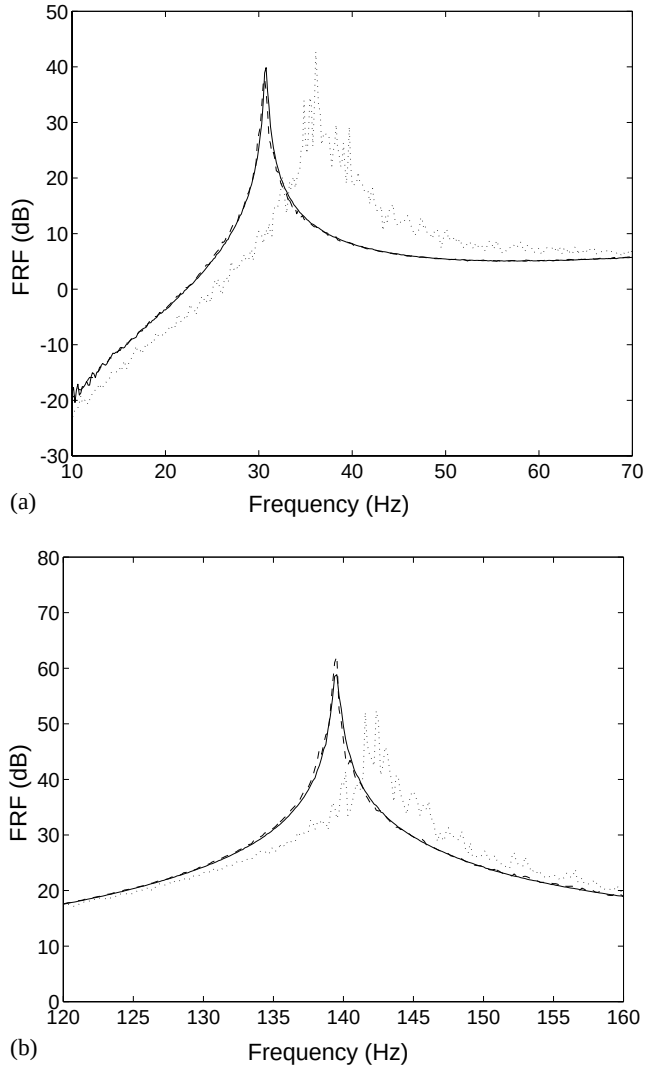

Fig. 13. Vertical set-up, magnitude of H_{73}. —, true FRF (1.4 N r.m.s.); ⋯⋯, H_2 estimate (22 N r.m.s.); - - -, H_{c2} estimate (22 N r.m.s.): (a) first resonance and (b) second resonance.

Table 4
Natural frequencies (H_{c2} estimate)

Excitation level (N r.m.s.)	First freq. (Hz)	Second freq. (Hz)	Third freq. (Hz)
Reference (1.4)	30.74	139.47	390.22
2.8	30.65	139.41	390.12
5.5	30.69	139.41	390.02
11	30.62	139.34	389.87
16	30.62	139.35	389.85
22	30.51	139.33	389.78

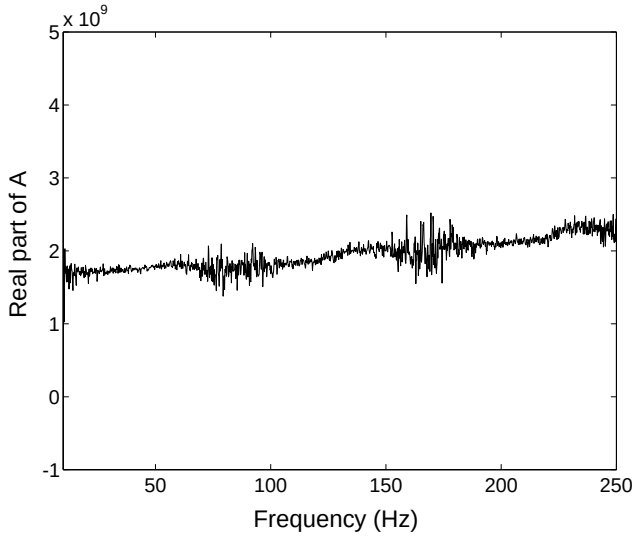

Fig. 14. Vertical set-up, real part of the non-linear coefficient (22 N r.m.s.).

Table 5
Spectral mean (10–250 Hz) of the non-linear coefficient

Excitation level (N r.m.s.)	A (N/m$^{2.8}$)
2.8	$2.69 \times 10^9 - \mathrm{i}2.76 \times 10^7$
5.5	$2.08 \times 10^9 - \mathrm{i}6.07 \times 10^7$
11	$1.94 \times 10^9 + \mathrm{i}1.09 \times 10^6$
16	$1.96 \times 10^9 - \mathrm{i}6.20 \times 10^6$
22	$1.96 \times 10^9 + \mathrm{i}1.55 \times 10^7$

the non-linear coefficient is identified. Again, the imaginary part of the coefficient is several orders of magnitude below the real part.

6. Conclusions

The aim of this paper has been to apply the CRP method to a non-linear beam. The non-linearity was realized by a thin beam excited with a large deflection. To evaluate the influence of gravity, two different set-up were built. Better results were obtained with the vertical set-up for which the influence of gravity is significantly reduced.

This work has also illustrated that the H_2 estimate is unable to recover the linear dynamic compliance functions of a m.d.o.f. non-linear system. Furthermore, the H_{c2} estimate, proposed by the CRP method, allows the distortions introduced in the FRFs by the non-linearities to be reduced. In a second step, the CRP method gives a reliable estimation of the non-linear coefficients. The key advantage of the method is its ability to deal with m.d.o.f. non-linear systems. In this context, it appears to be a useful method to be employed on more complex non-linear structures.

Acknowledgements

Mr. Kerschen is supported by a grant from the Belgian National Fund for Scientific Research (FNRS) which is gratefully acknowledged.

References

[1] S.F. Masri, T.K. Caughey, A nonparametric identification technique for nonlinear dynamic problems, Journal of Applied Mechanics 46 (1979) 433–447.
[2] M. Simon, G.R. Tomlinson, Application of the Hilbert transform in modal analysis of linear and non-linear structures, Journal of Sound and Vibration 90 (1984) 275–282.
[3] I.J. Leontaritis, S.A. Billings, Input–output parametric models for nonlinear systems, part I: deterministic nonlinear systems, International Journal of Control 41 (1985) 303–328.
[4] I.J. Leontaritis, S.A. Billings, Input–output parametric models for nonlinear systems, part II: stochastic nonlinear systems, International Journal of Control 41 (1985) 329–344.
[5] S.J. Gifford, G.R. Tomlinson, Recent advances in the application of functional series to non-linear structures, Journal of Sound and Vibration 135 (1989) 289–317.
[6] K. Worden, Nonlinearity in structural dynamics: the last ten years, Proceedings of the European COST F3 Conference on System Identification and Structural Health Monitoring, Madrid, Spain, 2000, pp. 29–52.
[7] F.M. Hemez, S.W. Doebling, Review and assessment of model updating for non-linear, transient dynamics, Mechanical Systems and Signal Processing 15 (1) (2001) 45–74.
[8] V. Lenaerts, G. Kerschen, J.-C. Golinval, Proper orthogonal decomposition for model updating of non-linear mechanical systems, Mechanical Systems and Signal Processing 15 (1) (2001) 31–43.
[9] T.K. Hasselman, M.C. Anderson, W.G. Gan, Principal component analysis for nonlinear model correlation, updating and uncertainty evaluation, Proceedings of the 16th International Modal Analysis Conference, Santa Barbara, USA, 1998, pp. 644–651.
[10] D.E. Adams, R.J. Allemang, A frequency domain method for estimating the parameters of a non-linear structural dynamic model through feedback, Mechanical Systems and Signal Processing 14 (4) (2000) 637–656.
[11] H.J. Rice, J.A. Fitzpatrick, A generalised method for spectral analysis of non-linear systems, Mechanical Systems and Signal Processing 2 (1988) 195–201.
[12] C.M. Richards, R. Singh, Identification of multi-degree-of-freedom non-linear systems under random excitations by the reverse-path spectral method, Journal of Sound and Vibration 213 (4) (1998) 673–708.
[13] J.S. Bendat, Nonlinear System Analysis and Identification from Random Data, Wiley, New York, 1990.
[14] J.S. Bendat, Spectral techniques for nonlinear system analysis and identification, Shock and Vibration 1 (1993) 21–31.
[15] V. Lenaerts, G. Kerschen, J.-C. Golinval, Identification of a continuous structure with a geometrical non-linearity. Part II: Proper orthogonal decomposition, Journal of Sound and Vibration, this issue.
[16] D.J. Ewins, Modal Testing: Theory, Practice and Application, 2nd Edition, Research Studies Press, Hertfordshire, UK, 2000.
[17] J.S. Bendat, Random Data: Analysis and Measurement Procedures, 2nd Edition, Wiley-Interscience, New York, 1986.
[18] C.M. Richards, R. Singh, Feasibility of identifying non-linear vibratory systems consisting of unknown polynomial forms, Journal of Sound and Vibration 220 (3) (1999) 413–450.
[19] Web-Site, http://www.ulg.ac.be/ltas-vis/costf3/costf3.html.
[20] G. Kerschen, V. Lenaerts, S. Marchesiello, A. Fasana, A frequency domain vs. a time domain identification technique for nonlinear parameters applied to wire rope isolators, Journal of Dynamic Systems, Measurement, and Control, Transactions of the American Society of Mechanical Engineers 123 (2001) 645–650.